Next-generation ALK inhibitors are highly active in ALK-positive large B-cell lymphoma

Supplementary Material

Table of Contents **Page Number**

Supplemental Table S1: Patient characteristics

	Patient 1	Patient 2	Patient 3	Patient 4
Age	50	50	50	25
Diagnosis	ALK-LBCL	ALK-LBCL	ALK-LBCL	ALK-LBCL
Biologic sex	3 male / 1 female			
At diagnosis				
Ann-Arbor Stage	4	3	4	4
ALK fusion protein	CLTC-ALK	N/A	N/A	CLTC-ALK
At alectinib initiation				
ECOG performance status	4	1	1	2
Stage	4	2	4	4
LDH	Elevated	Not elevated	Elevated	Elevated
≥2 extranodal sites	Yes	No	Yes	Yes
Number prior therapies (n)	8	2	2	3
Lines of therapy prior to alectinib administration	EPOCH (CR); DHAP (PD); Crizotinib (PD); Lenalidomide (PD); Bendamustine (PD); ICE (PD); Elotuzumab (PD); Gem-Ox (PD)	EPOCH (CR); ICE (CR) and HDT/ASCR	CHOP (PD); Crizotinib (PD)	EPOCH + Crizotinib (PD); Pembro (PD)
Relapsed or refractory to most recent therapy; DOR (if applicable)	Refractory	Relapsed; DOR, 3 months	Refractory	Refractory
Prior ALKi (best response)	Crizotinib (PD)	No	Crizotinib (PD)	Crizotinib (PD)
Prior HDT/ASCR	No	Yes	No	No

Supplemental Table S1: Patient characteristics at time of alectinib initiation. Baseline characteristics at diagnosis and at time of alectinib initiation are shown. Patient, disease characteristics and responses were tabulated and summarized descriptively. To protect patient identities, age is rounded to closest quarter-century, biologic sex is not reported on a patient level, and patient number is non-sequential. CLTC-ALK, t(2;17)(p23;q23) associated with fusion of ALK gene to clathrin heavy-chain gene; N/A, not available; LDH, lactate dehydrogenase; ALKi, ALK inhibitor; PD, progressive disease.

Supplemental Figure S1: Patient 1 response to crizotinib, alectinib, and lorlatinib

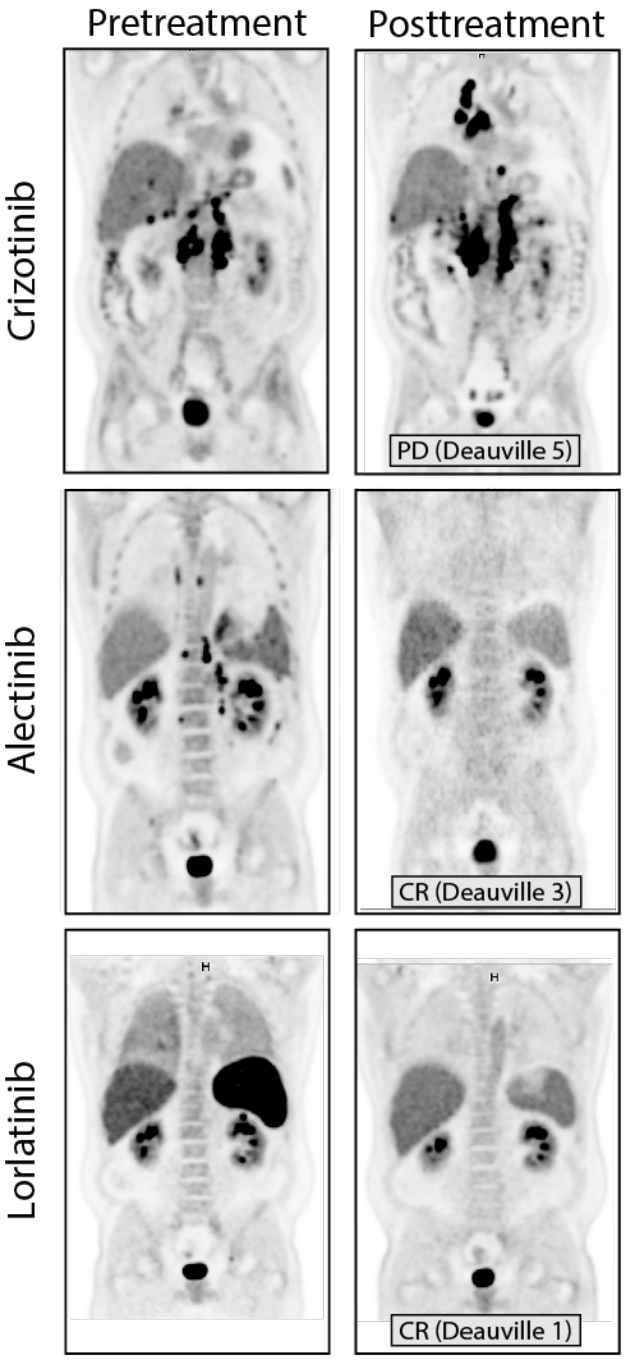

Supplemental Figure S1: Patient 1 response to crizotinib, alectinib, and lorlatinib. Maximum intensity projection FDG-PET images are shown pretreatment and at best response with sequential therapy on crizotinib (top), alectinib (middle), and lorlatinib (bottom), and posttreatment image is annotated with Lugano response and Deauville score. A detailed description of the patient's response to alectinib is provided (appendix p11). PD, progressive disease; CR, complete response.

Supplemental Figure S2: Patient 2 response to alectinib

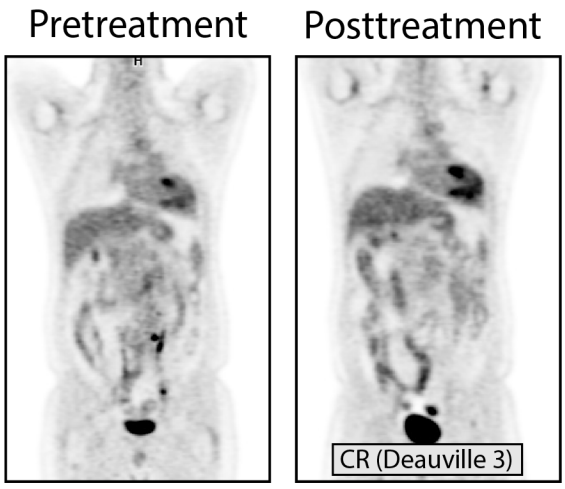

Supplemental Figure S2: Patient 2. Maximum intensity projection FDG-PET images are shown pretreatment and at best response with alectinib, and posttreatment image is annotated with Lugano response and Deauville score. A detailed description of the patient's response to alectinib is provided (appendix p11). CR, complete response.

Supplemental Figure S3: Patient 3 response to alectinib

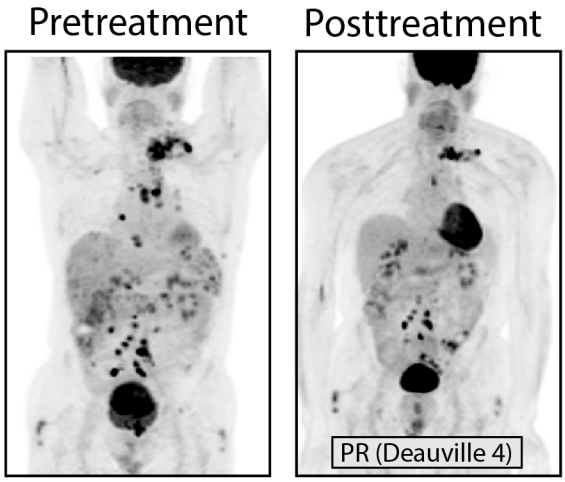

Supplemental Figure S3: Patient 2 response to alectinib. Maximum intensity projection FDG-PET images are shown pretreatment and at best response with alectinib, and posttreatment image is annotated with Lugano response and Deauville score. A detailed description of the patient's response to alectinib is provided (appendix p11). PR, partial response.

Supplemental Figure S4: Patient 4 response to alectinib

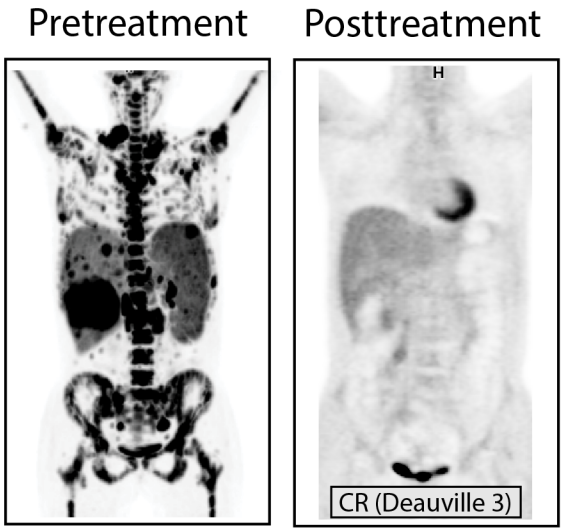

Supplemental Figure S4: Patient 4 response to alectinib. Maximum intensity projection (MIP) FDG-PET at best response shows Deauville 3 CR. Pretreatment MIP image is shown from one week prior to treatment demonstrating marked FDG uptake at all sites of lymphoma. CT imaging (not shown) was repeated prior to alectinib administration and demonstrated interval progression from pretreatment FDG-PET imaging to the pretreatment CT imaging. A detailed description of the patient's response to alectinib is provided (appendix p11).

Supplemental Figure S5: Ultrasound assessment of renal tumors in patient-derived xenografts

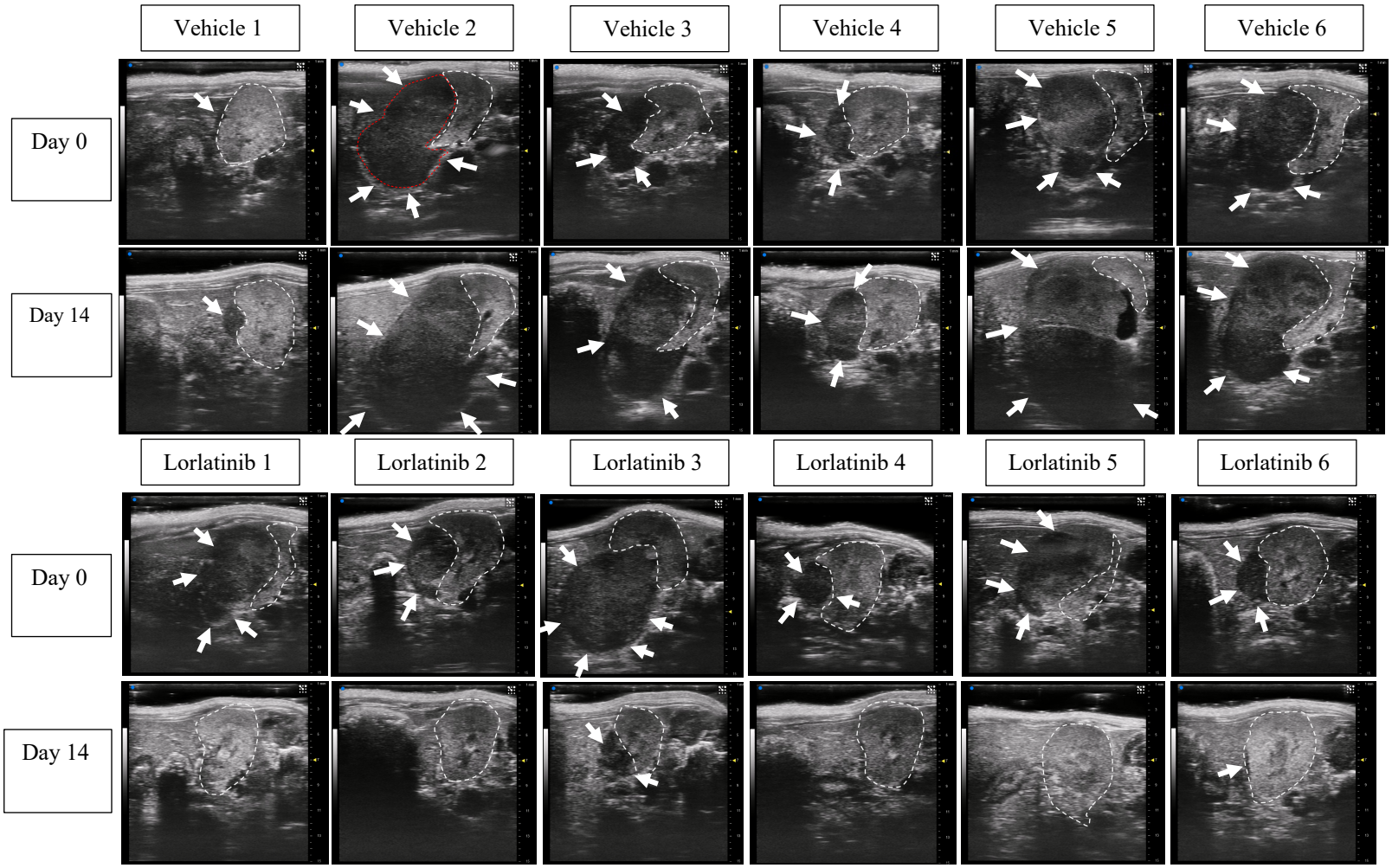

Supplemental Figure S5: Ultrasound assessment of renal tumors in patient-derived xenografts. ALK-positive large B-cell lymphoma (ALK-LBCL) patient-derived xenografts (PDXs) were created by implantation of tumor seeds underneath the renal capsule, resulting in tumor masses formed on the kidney surface. ALK-LBCL PDXs were treated with lorlatinib or vehicle (n=6 per group). This figure shows ultrasound images of the kidney tumors on Day 0 (prior to therapy) and at 14 days of daily treatment with either lorlatinib or vehicle. In these images the native kidney is outlined with dotted white line. Tumors are hypoechoic and tumor surface is delineated by white arrows. In all cases, PDXs treated with vehicle grew significantly in from Day 0 to Day 14. In contrast, PDX tumors treated with lorlatinib shrank significantly in all cases, and were completely absent in all but one case (Lorlatinib 3), which harbored a tiny residual tumor by 14 days, that was absent by 21 days (D21 time point not shown).

Supplemental Figure S6: Ultrasound assessment of renal tumors in patient-derived xenografts (video)

Future link to MP4 files (provided separately).

Supplemental Figure S6: Ultrasound assessment of renal tumors in patient-derived xenografts (video). Ultrasound assessments of representative renal tumor in patient-derived xenografts (PDX) at baseline, 7 days, and 14 days after treatment with lorlatinib 15mg/kg or vehicle (acidified water) are shown in video format.

Supplemental Methods

Western blotting. Tumors were lysed in GST buffer (10mM MgCl2, 150mM NaCl, 1% NP40, 2% Glycerol, 1mM EDTA, 25mM HEPES pH7.5), with protease inhibitors [1mM phenylmethylsulfonyl fluoride (PMSF), 10mM NaF, 1mM Na3VO4, and protease inhibitor cocktail (Millipore Sigma)]. Tumor lysates were incubated on ice for 2 hours and then centrifuged at 15000 rpm for 15 minutes at 40C. Supernatants were quantified using the BCA assay (Sigma). 50µg of protein was denatured at 950C for 5 minutes before gel electrophoresis on a 4-12% gel (BioRad). Proteins were transferred to nitrocellulose membranes at 75V for 60 minutes at 40C. We used the following antibodies: pALK^{Tyr1604} (Cell signaling #3341), pALK^{Tyr1278} (Cell signaling #6941), ALK (Cell signaling #3633), STAT3 (Cell signaling #12640), pSTAT3^{Tyr705} (Cell signaling #9145), SHP2 (Cell signaling #3397), pSHP2^{Tyr542} (Cell signaling #3703), Beta-actin (Sigma # A5316).

Targeted DNA and RNA sequencing. Anchored Multiplex PCR enrichment was used for clinically validated targeted DNA sequencing (heme/solid-SnaPshot assays) for Single nucleotide variants (SNVs) and insertion/deletion variants (indels) and targeted RNA sequencing (heme-fusion assay) for fusion transcript detection, using ArcherDx primers. Illumina NextSeq 2x150 base paired-end sequencing results were aligned to the hg19 human genome reference using bwa-mem for fusion detection and Illumina Novoalign followed by an ensemble variant calling approach, using MuTect1 LoFreq, GATK and a laboratory developed hotspot caller for SNV and indel variant detection. A laboratory-developed algorithm was used for fusion transcript detection/annotation.

Fluorescence *in-situ* hybridization (FISH). Break-apart probes for ALK rearrangements (Kreatech ALK Breakapart FISH Proximal Green and Distal Red probes), and KRAS copy number changes (Abnova, Taipei City, Taiwan), were hybridized (formalin-fixed paraffin-embedded tumor material) and used to calculate the number nuclei of 50 scored containing a rearrangement or increased gene-specific probe-to-centromere ratio. An ALK rearrangement was reported if >15% cells showed split signals and confirmed with an ALK break-apart probe (Vysis LSI ALK (2p23) Dual Color). A KRAS-to-centromere 12 ratio of >2.2 was considered positive for KRAS gene amplification.

Whole exome and RNA sequencing. Tumor biopsies from one patient and a matched PDX derived model were processed for RNA-Seq and WES. Germline WES was derived from the patients' skin biopsy. Tumor RNA was isolated using the AllPrep DNA/RNA Mini kit (Qiagen) and libraries were generated using the Stranded mRNA Prep kit (Illumina). Tumor DNA was isolated using the AllPrep DNA/RNA Mini kit (Qiagen) and libraries were generated using the SureSelect XT HS2 DNA Library construction kit (Agilent). Normal DNA was extracted from a saliva sample by Maxwell® RSC Stabilized Saliva DNA Kit (Promega) and libraries were generated using the SureSelect XT HS2 DNA Library construction kit (Agilent). Paired end sequencing was performed on a NovaSeq6000 with a sequencing depth of 50M reads (2 X 150 pairs).

Quality control for NGS data. Quality control was performed by FastQ Screen [Wingett SW te al] and FASTQC [Available online at: http://www.bioinformatics.babraham.ac.uk/projects/fastqc/], and summarized using MultiQC tool [Ewels P et al]. For sample correspondence HLA profiling and polymorphism (SNP) comparisons were performed: HLA were detected by optitype [Szolek A et al] and SNP were compared by Conpair [https://github.com/nygenome/Conpair].

RNA-Seq data processing. RNA-seq reads were mapped to the GENCODE v23 reference transcriptome [Achuthan P et al] by Kallisto aligner [Bray NL et al]. Next, only coding transcripts were kept - in total 20,062 transcripts. And read counts were transformed in TPM, summarized by genes and log2 transformed. For the PDX sample xengsort algorithm [Zentgraf J et al] was used to split reads into human, mouse or neither origin. Gene expression was calculated by combining host and graft raw Kallisto output and refactoring TPM values.

B-cell receptors (BCR) reconstruction was performed by MiXCR v3.0.12 [Bolotin DA et al]. To capture somatic hypermutations in malignant B-cells all the related BCR clonotypes sharing the same V(D)J segments and similar CDR3 sequences were combined into clonotype groups.

Fusions were detected by STAR-fusion [Haas B et al] and next evaluated by the FusionInspector module.

Single gene expression levels were calculated and shown relatively to their expression level in DLBCL patients (NCICCR N=567 samples [Schmitz R et al] and NCICGCI N=104 samples [Morin et al.]). For rank calculation, thresholds were used as follows: low was for expressions below 17 percentile, high was for above 83 percentile, the rest were medium.

Cell composition was reconstructed using Kassandra BG Algorithm [Zaytcev A et al], LME DLBCL transcriptomic subtypes and ABC/GCB COO were determined by previously published method [Kotlov N et al].

WES data processing. Reads were mapped to the human reference genome GRCh38 by BWA v0.7.17 [Li H.]. Xengsort was used for PDX samples' reads filtration into human, mouse and other origin [Zentgraf J et al].

For somatic and germline mutation GATK v4.1.2.0 pipeline was used [Van der Auwera GA et al]. In brief, FilterByTile/BBMap was used for Low-quality reads filtration, Mark Duplicates was used for duplicate reads excluding, IndelRealigner and BaseRecalibrator were used for accurate indels re-alignment and calling. Next, germline and somatic variations were identified by Strelka [Kim S et al] and annotated by the Variant Effect Predictor [McLaren W et al].

The clonal/subclonal status of events was based on WES from the tumor and a normal control. For this we incorporate the copy number, as well as other features (e.g. coverage of reference, alternative allele), of detected somatic mutations in the tumor sample. BostonGene custom approach (based on McGranahan N et al) could classify each of the somatic mutations as clonal or subclonal and thus decipher the core of the Clonal mutations based on their VAF (variant allele frequency that is equal to the ratio between alternative allele coverage and total allele coverage) and Copy number status. The revealed mutation profile corresponds to the estimated tumor cellularity and CNA ploidy profile. Low covered somatic mutations are excluded from the clonal composition analysis. Copy number alterations (CNAs) were calculated using a modified version of FACETS [Shen R et al] and Sequenza (version 2.1.2) [Favero F et al] callers. Microsatellite status was evaluated by MSIsensor2 (v0.6) [Niu B et al].

Supplemental Results: Pathology review of four patients

Pathology review of each of the four cases revealed tumors comprised of sheets of large malignant lymphoid cells with plasmablastic morphology and ALK expression. In all cases, neoplastic cells lacked expression of B and T cell antigens (CD20, CD19, PAX5, CD3, CD2, CD5). Two tested cases confirmed characteristic strong expression of IgA and CD4. Two tested cases showed evidence of *CLTC-ALK* fusion.

Supplemental Results: Detailed description of patient responses to alectinib

Patient 1

Patient 1 was a 50-year old diagnosed with ALK-positive large B-cell lymphoma (ALK-LBCL), who was refractory to eight prior therapies, including crizotinib, when he was admitted with abdominal pain, peritonitis, and septic shock, prompting emergent exploratory laparotomy. Intraoperatively, the surgeons observed murky peritoneal fluid with studding throughout the peritoneum and bowel, necrotic distal transverse colon, and a large abscess at the splenic flexure. He underwent subtotal colectomy, and surgical pathology confirmed extensive mural, pericolonic, and omental involvement by ALK-LBCL, resulting in transmural perforation of the colon. On postoperative day (POD) 2, the patient had worsening lymphoma-related pain as well as post-operative pain. Alectinib was initiated on POD 2, the patient's lymphoma-related pain improved in <24 hours, and he was discharged home on POD 16. His lymphoma symptoms resolved and PET-CT imaging on day 27 confirmed complete response (CR) (Deauville 3). PET-CT imaging was repeated prior to planned conditioning for allogeneic stem cell transplantation (49 days after initiation of alectinib), which demonstrated progressive disease (PD; duration of response [DOR] 1.6 months). The third generation ALK inhibitor lorlatinib was administered at 100 mg PO once daily as off-label treatment. Remarkably, the patient's lymphoma symptoms resolved within days of initiation and PET-CT on day 15 confirmed CR (Deauville 1). PET-CT was repeated on day 30 and demonstrated PD (Deauville 5; DOR 1 month).

Patient 2

Patient 2 was a 50-year-old diagnosed with ALK-LBCL who had recurrent disease within 3 months of completing high dose therapy and autologous stem cell rescue (HDT/ASCR) following second-line chemotherapy. Alectinib was initiated. His lymphoma symptoms resolved and subsequent PET-CT on day 43 of alectinib demonstrated PR (Deauville 4) with mild residual uptake in a partially calcified, 1.1 cm, retroperitoneal lymph node. They underwent allogeneic SCT (matched related donor) on day 89 from alectinib initiation and had no significant transplant-related morbidity and no graft-versus-host disease. Alectinib was held on the day of admission for pretransplant conditioning (busulfan 3.2 mg/kg and fludarabine 30 mg/m^2) and resumed 59 days posttransplant. The patient is in an ongoing CR (Deauville 3) at 22.3 months post alectinib initiation and remains on alectinib (DOR 22.3 months).

Patient 3

Patient 3 was a 50-year-old diagnosed with ALK-LBCL who achieved transient clinical benefit with second line crizotinib but developed progressive pain from multifocal osseous disease and PET-CT confirmed PD (Deauville 5). Alectinib was initiated. The patient reported rapid improvement in his pain and PET-CT on day 28 demonstrated PR (Deauville 4). The patient subsequently developed sacral pain and PET-CT on day 56 of alectinib showed PD (Deauville 5; DOR 1.8 months).

Patient 4

Patient 4 was a 25-year-old with ALK-LBCL refractory to three prior therapies including crizotinib. The patient had high disease burden including rapidly progressive subcutaneous masses and palpable adenopathy. Alectinib was initiated. The patient demonstrated resolution of the subcutaneous masses within one week, and FDG-PET and CT on day 15 confirmed PR (Deauville 4) and decrease in the dominant liver mass (10.7x12cm to 7.6x8.2cm) and spleen size (21.9cm to 16.8cm). The patient received consolidation with 1 cycle of daratumumab/hyaluronidase-fihj with alectinib, then underwent allogeneic SCT (matched unrelated donor), is in ongoing CR (Deauville 3) at 7.2 months post alectinib initiation and remains on alectinib (DOR 7.2 months).

Supplemental Results: Molecular characterization of PDX and original tumor

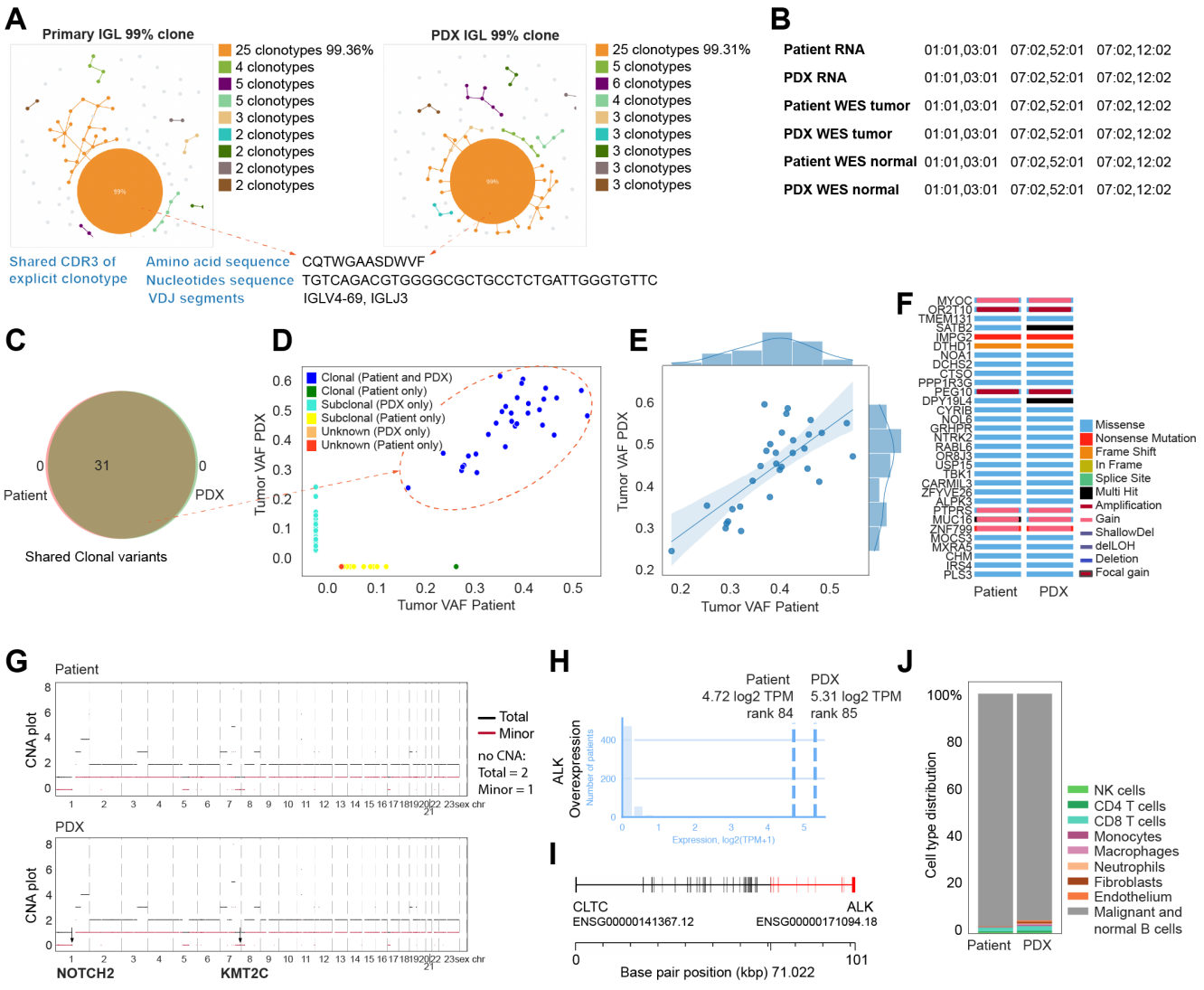

Supplemental Results: Molecular characterization of PDX and original tumor. (A) Analysis of IG lambda clonality by RNASeq is shown. Clonal composition map shows IGL structure, with each node corresponding to a unique CDR3 and its size corresponding to clonotype coverage. We found large (99% reads coverage) explicit tumor clonotypes in the IG lambda chain with identical CDR3 in both the patient and PDX samples. Heavy and kappa IG chains had low coverage in both samples. (B) Analysis of HLA haplotype for the patient and PDX samples are shown. We found that the patient and PDX samples exhibited the same HLA haplotype (HLA-A 01:01,03:01; HLA-B 07:02,52:01; HLA-C 07:02,12:02) supporting shared origin. (C) A Venn diagram demonstrating clonal somatic mutations observed in the patient and PDX is shown. We observed that the patient and PDX samples exhibited complete overlap in clonal somatic alterations (n=31). (D) A scatter plot depicting somatic mutations by patient (x-axis) and PDX samples (y-axis) is shown. Clonal mutations were shared between patient and PDX samples, while subclonal mutations were not. (E) A scatter plot depicting correlation of variant allele frequencies by patient (x-axis) and PDX samples (y-axis) is shown. Variant allele frequencies of shared mutations showed high correlation (r = 0.73, p-value = 2.6e-06). (F) An Oncoplot for the 31 shared somatic mutations is shown. (G) Copy number alterations landscape is shown for the patient (top) and PDX (bottom) samples, with the black line representing total number of copies and red line representing the number of copies of the minor allele. We observed high similarity between the patient

and PDX samples, although we found complete loss of *NOTCH3* and *KMT2C* in the PDX sample, while in the patient sample one copy for each of the genes were left. (H) ALK expression in the patient and PDX samples is shown relative to a cohort of 671 cases of diffuse large B-cell lymphoma (DLBCL). We observed high ALK expression in the patient (4.72 log2 tpm with rank 84%) and PDX samples (5.32 log2 tpm with rank 85%) compared with the DLBCL cohort (0.085 log2 tpm). (I) CLTC-ALK transcripts are shown for the patient and PDX samples. The x-axis represents genomic coordinates. An identical fused CLTC-ALK transcript was found in the patient (supported by 615 junction reads, 60 spanning reads) and PDX samples (191 junction reads, 14 spanning reads). (J) Cell composition reconstruction based on RNA-Seq is shown for the patient and PDX samples. Tumor content was 97% in the patient sample and 95% in the PDX sample. CD8 T-cell content was 1.5% in the patient sample and 2% in the PDX sample. All other populations were less than one percent.

Supplemental Results: QC for whole exome sequencing of PDX and original tumor

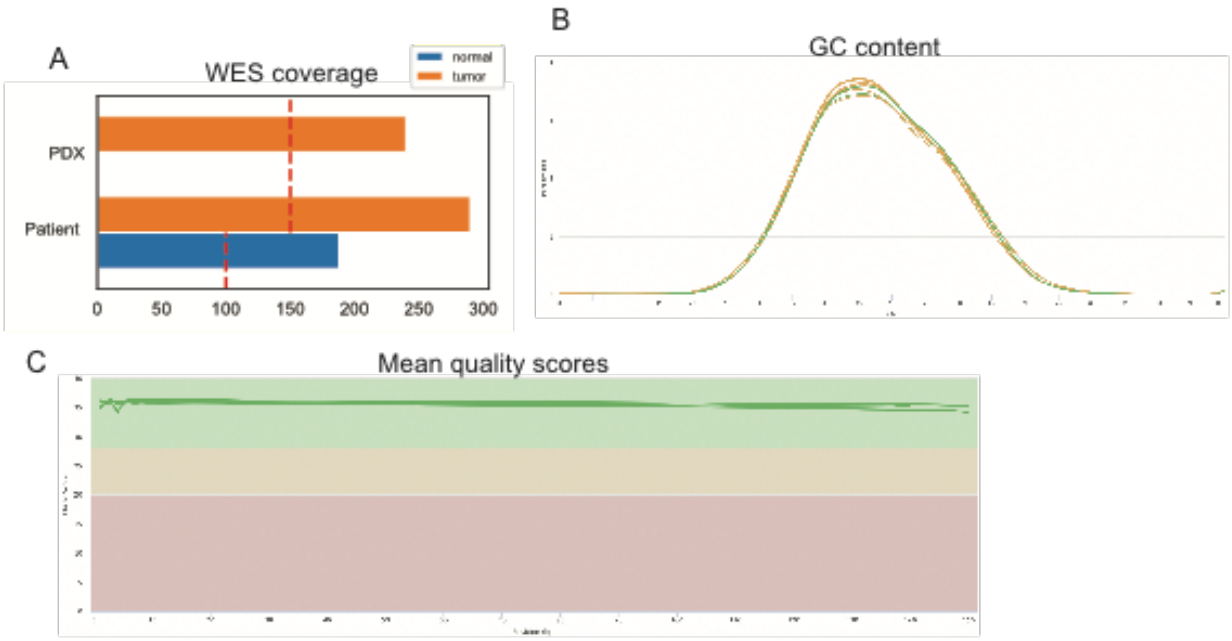

Supplemental Results: QC for whole exome sequencing of PDX and original tumor. (A) Normal and tumor median WES coverage are shown, with the x-axis representing number of millions of reads. (B) Mean quality of reads (WES) according to FastQC results is shown, with green depicting good quality. (C) GC content (WES) according to FastQC results is shown. In summary, we observed high coverage with median 188x in germline sample, 290x in the patient tumor sample and 240x in the PDX tumor sample. Read quality was good, GC content was similar. Low duplication level.

Supplemental Results: QC for RNA sequencing of PDX and original tumor

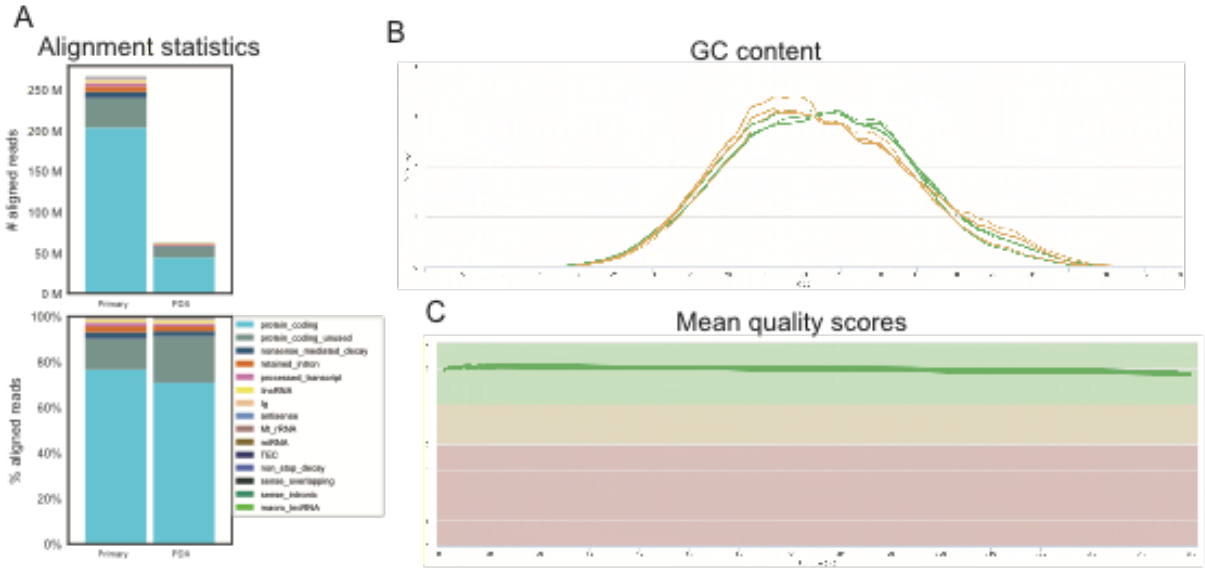

Supplemental Results: QC for RNA sequencing of PDX and original tumor. (A) Read alignment statistics of RNA-Seq according to the Kallisto results are shown, with color corresponding to different transcript types. (B) Mean quality of reads (RNA-Seq) according to FastQC results is shown, with green depicting good quality. (C) GC content (RNA-Seq) according to FastQC results is shown. In summary, we observed high coverage (50M aligned reads for the PDX and 234M reads for the patient sample) with more than 70% reads mapped for protein coding transcripts in both samples.

Supplemental Results: Targeted DNA sequencing of crizotinib-refractory ALK-LBCL

Patient 1	**Pre-crizotinib biopsy**	**Post-crizotinib/pre-alectinib biopsy**
Cytogenetics	46,XY[5].nuc ish(ALKx3)(3'ALK sep 5'ALKx2)[5/50]	Not done
ALK FISH	Positive for ALK rearrangement; nuc ish (ALK x 2) [44/50]; no ALK amplification	Positive for ALK rearrangement; nuc ish (ALK x 2) [44/50]; no ALK amplification
KRAS FISH	Negative for KRAS rearrangement or amplification	Failed QC
Targeted gene fusion assay	CLTC Exon31 and ALK Exon20 (490 reads)	CLTC Exon31 and ALK Exon20 (606 reads)
Targeted DNA sequencing (Heme SNaPshot)		TET2 ENSP00000369351.4:p.Gln1084Pro 19.8% KMT2C ENSP00000262189.6:p.Pro792Leu9.7% PPM1D ENSP00000306682.2:p.Lys469Glu 17.8%
Patient 4	**Pre-crizotinib biopsy**	**Recurrence 1 (focal liver biopsy)**
Cytogenetic analysis	N/A	Not done
Targeted gene fusion assay		CLTC Exon31 and ALK Exon20 (445 reads)
Targeted DNA sequencing and copy number analysis (Oncopanel)		ALK intron 19 (chr2:29446540):: CLTC intron 31 (chr17:57769076); two copy loss of ID3; no ALK or KRAS amplification